IEEE Access
Multidisciplinary ⋮ Rapid Review ⋮ Open Access Journal

Received 19 September 2023, accepted 8 November 2023, date of publication 16 November 2023,
date of current version 27 November 2023.

Digital Object Identifier 10.1109/ACCESS.2023.3333367

RESEARCH ARTICLE

A Novel Method for Optimizing Color Selection Using the Hadamard Product Technique

TONI KUSNANDAR, JUDHI SANTOSO, AND KRIDANTO SURENDRO, (Member, IEEE)
School of Electrical Engineering and Informatic, Institut Teknologi Bandung (ITB), Bandung 40132, Indonesia
Corresponding author: Toni Kusnandar (33220008@mahasiswa.itb.ac.id)

This work was supported by the Institut Teknologi Bandung (ITB).

ABSTRACT Numerous research endeavors have employed color selection procedures for a vast array of purposes. Detecting defects in fabrics, calculating the Microbial Community Color Index, analyzing digital color to facilitate fashion design processes, applying color to artworks, calculating canopy cover, and achieving other objectives have been the subject of research. This procedure requires intricate steps, calculations, and a lengthy computational time. In this study, a novel strategy for optimizing the color selection process using the Hadamard product technique is presented. The HSV color space is optimized by selectively selecting the desired colors and establishing threshold limits for each hue, saturation, and value component. The optimization results demonstrate that the desired colors are perfectly distinguished from other colors. Additionally, the proposed method employs a straightforward, step-by-step procedure that does not require feature extraction. In comparison to previous research, a remarkable increase in computational speed of 1,078.82 times faster has been observed. This improvement is achieved by multiplying each element of the HSV matrix resulting from color selection as opposed to the HSV matrix without selection. The faster computational speed observed in this study during the color selection process has the potential to be used in unmanned aerial vehicles to select green plants or ripe fruits.This study's findings are applicable not only to plant images but also to all cases requiring color selection under visible light conditions.

INDEX TERMS Color selection, color space, Hadamard product, Heaviside step function.

I. INTRODUCTION

Computer vision requires the detection of foreground objects in scenes, and the color space (CSP) used is crucial. Grayscale and RGB CSP are not always the best for detecting foreground objects, especially in dynamic backgrounds [1]. In the traditional method of choosing colors for packaging design, there is no good match between the image and the colors, and users are unhappy with the results [2]. The color, material, texture, and shape of an object affect how we perceive it [3]. Segmenting an image is a well-established method for isolating a particular object in a picture. There are three components of the human visual system that contribute to the perception of color. This concept is utilized by color display devices, which generate their entire color palette by combining the three primary hues. With the aid of these primary colors, any visible hue can be created [4].

The associate editor coordinating the review of this manuscript and approving it for publication was Jeon Gwanggil.

Low-quality image segmentation is a common issue in food recognition and estimation [5]. Animals that forage visually use color as an important cue in the detection and acquisition of food, especially insects. It is possible to use color to judge whether a food source is suitable, improve the effectiveness of food detection, and even guide the choice of a mate [6].

The color selection (CS) method has been utilized in numerous studies for a wide variety of purposes. Utilizing CS techniques to address issues of noise and blurriness in original fabric images, research has been conducted to detect defects in fabrics. Enhancing the contrast between flaws and the background is the strategy. Utilized preprocessing methods include CSP fconversion, Gaussian filtering, saliency map generation, and contrast stretching [7]. In addition, CS processes are used to calculate the Microbial Community Color Index (MCCI). Analyzing images involves considering circular regions of varying diameters. At each pixel, the RGB channel intensities (red, green, and blue) are extracted to

generate an artificial color scale resembling the original filter colors. This fabricated scale is then used to calculate the MCCI [8]. CS is also performed for digital color analysis in order to facilitate the fashion design process and the use of artistic colors in fashion product design [9]. Greenness identification in crop images is crucial for monitoring growth. Common methods use the visible spectral index, assuming plants display high greenness with soil as a background. Brightness and contrast are affected by weather and capture time [10].

A piecewise defined function is a key concept in operational calculus, applied, and engineering mathematics. This can be performed in a simple manner using algebraic representations [11]. Modeling the discontinuity of the displacement of the element, including the crack tip or front, with the Heaviside function and a step function, is possible [12]. The Heaviside step function (HSF) is used by Huo and Yu to study how decision-adoption affects layer transmission. The differences in self-recognition and physical quality are assumed to be Gaussian [13].

A method for interacting with features based on the Hadamard product (HP) can integrate multimodal features better than the dot product and give a rich representation of features [14]. Infrared small target detection faces challenges due to complex backgrounds and noises, making it challenging for long-distance applications. A fast, reliable method using HP for spatial-temporal matrices (HPSTM) is proposed by Ping-Hsiu Wu et al. for improved accuracy and efficiency [15]. Spatial smoothing improves the subspace method's performance in coherent sources, but it also increases the array size needed to detect the sources. From the perspective of an HP, Yang et al. discuss the source resolvability of spatial-smoothing-based subspace methods [16].

Based on Scopus database, related research CS is still commonly found (4,770 document) with a trend as can be seen in FIGURE 1.

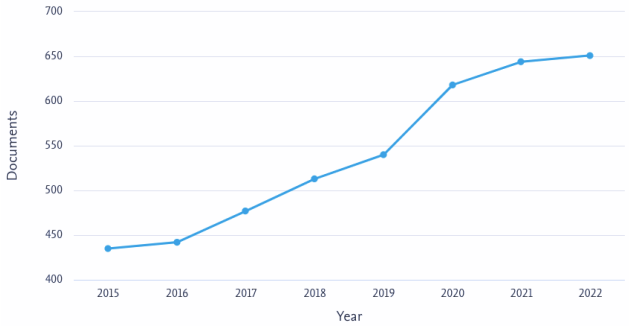

FIGURE 1. Related research CS.

As can be seen in FIGURE 2, the vast majority of CS research carried out with the aid of the Scopus database is classified as belonging to the field of engineering and computer science. In the field of computer science, there have been a total of 1031 research papers published, whereas there have been 3,339 research papers published in the field of agricultural and biological sciences. According to the information presented in Table 1, Agricultural and Biological Sciences, Computer Science, Biochemistry, Genetics and Molecular Biology, Engineering, and environmental science are among those with the highest levels of research activity. There were 431 CS studies published between January 2023 and August 2023. The fields of agriculture and biology accounted for approximately 35.2 percent of the research, while the field of computer science accounted for approximately 14.8 percent of the research. 450 papers were published between 2013 and early September, as shown by the Scopus database. There were 320 publications in the field of Agricultural and Biological Sciences, 135 in the field of Computer Science, 87 in the field of Engineering, 84 in the field of Biochemistry, Genetics, and Molecular Biology, and 53 in the field of Environmental Science.

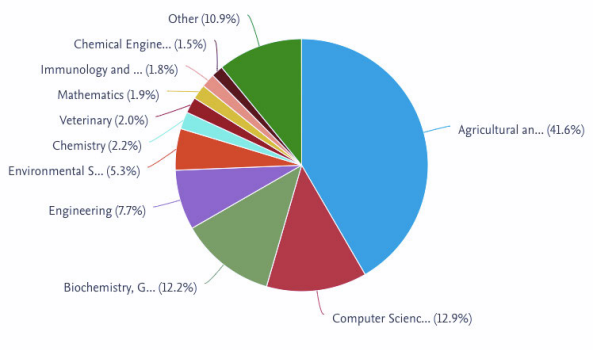

FIGURE 2. Research CS on year 2015-2022.

TABLE 1. Research CS on year 2015-2023 by subject area.

Subject area	Documents
Agricultural and Biological Sciences	3,339
Computer Science	1,031
Biochemistry, Genetics and Molecular Biology	979
Engineering	616
Environmental Science	426
Chemistry	176
Veterinary	163
Mathematics	153
Immunology and Microbiology	142
Chemical Engineering	122
Materials Science	119
Physics and Astronomy	119
Neuroscience	115
Medicine	103
Social Sciences	101
Earth and Planetary Sciences	55
Health Professions	49
Multidisciplinary	44
Decision Sciences	30
Nursing	29
Energy	25
Business, Management and Accounting	23
Arts and Humanities	22
Psychology	21
Pharmacology, Toxicology and Pharmaceutics	10
Economics, Econometrics and Finance	7
Dentistry	1

The primary result of this study is a novel application of the HP method for optimizing CS. Previous studies that only used

hue parameters to select green in the HSV color space (HSV) in plant images can be enhanced with the findings of this study [17]. Due to the separation of color channels, intensity channels, and saturation channels, the HSV is still used for this optimization. Given that a key characteristic of healthy photosynthesis is increased green reflectance [18], [19], [20], this study begins by filtering only green light. The median hue value for green is approximately 120°, but for the purposes of this study, the hue range 90° to 150° is selected. The heavyside step function (HSF) is utilized during the color separation procedure in the HSV. The optimization results for picking green or any other color are flawless, as none of the less desirable hues are kept after the process.

In addition, the amount of time required for computation is drastically cut down thanks to this optimization, going from two to three minutes down to just 0.2 to 0.3 seconds. This increase in computational speed is achieved by employing the HSF method to perform element-wise multiplication using the Haddard Product (HP) technique. This allows for a greater degree of flexibility.

II. RELATED WORKS

The colors we see come from light waves that are reflected by objects. The source of the light and the way the objects reflect light affect the colors we see [21]. Ansari and Singh highlight the importance of CSPs in representing images, as they are a robust descriptor. Real-time algorithms' performance relies on selecting appropriate CSPs like RGB, nRGB, HSV, TSL, YCbCr, YUV, YES, CIE-XYZ, and CMYK [4]. In order to improve the aesthetics of product packaging, Fan suggests using particle swarm optimisation to select the right colors. The method calculates colour intelligent selection parameters based on hue values, constructs an objective function, and uses particle swarm optimisation to optimize parameters. The method adjusts brightness and enhances detail contour, completing intelligent CS [2].

Bhunia et al. developed a novel text recognition method using color channels for scene images and video frames. The system uses HMM and Pyramidal Histogram of Oriented Gradient features. The method analyzes image properties and applies a multi-label SVM classifier to select the best color channel for optimal recognition [22].

FGCC is a non-destructive, easy-to-measure variable used in ecology, environmental science, and agronomy. Canopeo, a Matlab program, uses the ACT algorithm to analyze and categorize pixel values based on R/G, B/G, and excess green index ratios. It finds FGCC faster and more accurately than other software packages. However, Canopeo requires aerial photographs or specialized equipment for vegetation exceeding 2.5 meters [23]. Córcoles et al. used UAV-collected images to derive canopy cover measurements and differentiate plant green colors from soil, shadows, and rocks. The k-means method was used to analyze color clusters, but the process became less computationally efficient when applied to the entire image [24]. Scientists use the GLI vegetation index for monitoring plant harvesting in farms and forests. It analyzes visible spectrum bands captured by RGB cameras, providing better results for each unique orthophoto. The index is applicable to any RGB orthophoto, regardless of the situation [25].

Plant stand count measures yield, efficiency, and seed quality, reducing manual measurement time and error. UAV-generated high-resolution images and computer vision algorithms directly influence yield. Automatic multiresolution Retinex correction reduces lighting effects in color images, enhancing multivariate linear models' performance [26]. Fundus images can be corrected for uneven contrast and luminosity using a five-step process: image input, selection, luminosity correction, histogram stretching, and post-processing [27].

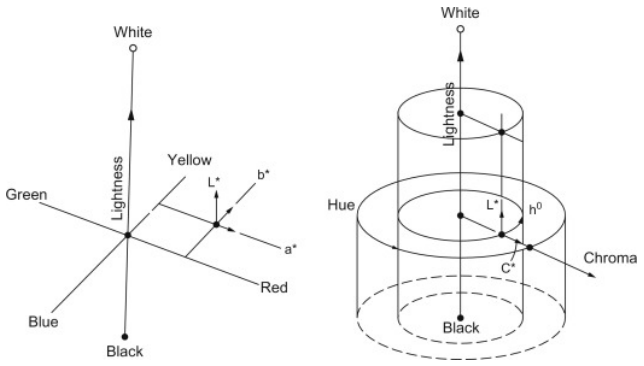

FIGURE 3. A three-dimensional graph depicting the brightness, chroma, and hue of actual surface colors [28].

In studies of the perfect reflectance method, it has been determined that accurate reflectance data is generated by objects with effective light reflection [29]. Digital images' light reflectance is determined using CSPs, mathematical representations of colors, derived from RGB data from cameras and scanners. RGB is the most popular CSP for computer images [19]. The transformation of CSPs is a fundamental aspect of image processing and a crucial aspect of observing the real world through camera equipment [30], [31]. CSP transformation aims to faithfully reproduce data from the physical world without altering it, using various models to extract relevant data based on application requirements [30]. However, such transformations frequently result in the loss of information. Some examples of CSP transformations that result in loss of information include printing in grayscale, converting multispectral or multiprimary data to tristimulus space, and converting between color gamuts [32]. Image data is transformed from RGB space to various CS like LHS, HSI, YIQ, HSV, ensuring intensity and saturation without altering hue, despite potential gamut problems [33].

CSP systems can precisely describe color stimuli. Multiple color systems, including RGB, CMYK, and CIELAB, are utilized. FIGURE 3 depicts a three-dimensional representation of a CSP with luminance along one axis, chroma along another axis, and a hue circle where hue is measured in degrees. This configuration provides a reasonable color scale

in terms of luminance and chroma, while scaling along the hue circle is relatively consistent [28].

Research conducted by Deng et al. proposed a new method to enrich crack fronts using the extended finite element method (XFEM). They combined HSF to model uneven displacement, eliminating the need for geometrical characteristic lengths. The step function activates discontinuity based on level set function [12]. According to Sivavelu et al., the KMO correlation test is useful for comparing test and training data. The new Heaviside step activation function analyzes KMO correlation test results to predict software faults [34]. The four-node plate element is used for finite element formulations, as discovered by Yan Guo et al., who found that Langrage interpolation functions are used for structural unknowns that lie outside the plane of the element, and Hermite cubic interpolation functions are used for structural unknowns that lie within the plane of the element. The delamination is modeled using HSF, which accommodates discontinuity in displacement fields [35].

Image algebra, based on heterogeneous algebra, offers a rigorous mathematical environment for computer vision algorithm development, comparison, and optimization [36]. Element-wise multiplication, also known as HP, is an often-overlooked concept in matrix theory for element-by-element multiplication [37], [38]. Element-by-element matrix multiplication is fundamental in matrix computations, especially in matrix differentials, with HP being a notable example [39]. Due to the element-by-element nature of the multiplication, matrices must be of identical size when employing this operation [37]. For the purpose of controlling the connection coefficients of the state variables of the systems, a new model that is formulated in terms of the HP has been suggested. A HP involving bilinear matrix inequalities is used to derive the control law that will stabilize the systems through the regulation of connection coefficients. This law is obtained in this manner [40].

Dehazing images has grown in recent years, with deep learning techniques showing improved performance. A novel HP model using data-driven priors and Learnable Hadamard-Product-Propagation (LHPP) mitigates noise and artifacts for optimal output [41]. According to the findings of a study that was carried out by Omran et.al., the HP of real symmetric positive definite matrices is a necessary condition for a theorem of Banach's on fixed points in a generalized metric space. This yields superior results to those of Perov because it does not require the condition that a matrix A converges to zero [42]. Yang et al. propose CNMF-HP to estimate 2-DOF wrist movements (flexion/extension; adduction/abduction) from myoelectric signals. This algorithm combines HP and constrained NMF [43].

In Table 2, we can see five relevant studies discussing CSP for different applications and research approaches. UAVs and other visible-light cameras were used in its implementations, and it was put to use on a number of different types of objects.

The use of drones, also known as unmanned aerial vehicles (UAVs), provides significant benefits to precision agriculture by reducing labor needs and achieving significant time savings [45], [46]. UAV image capture is more effective and user-friendly [47]. Using new UAV technology, Oakes and Balota investigate the effect of seeding rate on peanut varieties. High-yielding varieties increase profit without incurring additional input expenses, whereas the seeding rate determines input expenses. Using UAV indices, the study aims to measure emergence, seeding rate, growth rate, and potentially yield predictions [44]. Gilad Weil et al. found a cost-effective phenology-based approach for optimizing UAV imagery acquisition. A camera that is placed on the ground produces yearly time series of nine spectral indices and three color conversions from data collected at four different locations in the East Mediterranean that have distinct environmental conditions. This method does not consider cost-benefit or the ability to apply it to larger areas with more natural heterogeneity [48]. The proposed method will strengthen the benefits of using UAVs in agriculture by enabling real-time identification processes, which will allow for quick calculations, and by providing quick solutions.

TABLE 2. An overview of the prior research.

Paper Source	Author	Year	Dataset	Method	Novelty/Result
[10]	W. Yang et al.	2015	The leaves of maize seedlings range from dark to bright green.	HSV decision tree-based greenness identification from outdoor maize seedling images.	Proposed method accurately identifies greenness pixels in outdoor crop images.
[1]	López-Rubio et al.	2016	video sequences from various places	Proposed CSP and weighting selection process for foreground object detection.	Benchmark videos reveal experimental results.
[44]	Oakes and Balota	2017	UAV-captured RGB and NIR peanut images.	Examine how seeding rate affects peanut varieties.	In early planting weeks, aerial indices distinguish seeding rates and emergence, but not peanut yield prediction, making them unsuitable for later-season use.
[22]	Bhunia et al.	2018	4,947 word images for scene and 4,848 for video text recognition.	Text recognition employs Pyramidal Histogram, Oriented Gradient features, and Hidden Markov Model.	An innovative color channel selection method for scene image and video frame text recognition.
[2]	Fan et.al.	2023	Packaging design image	New product packaging color intelligent selection using particle swarm optimisation algorithm	The method improves product packaging CS, resulting in satisfaction scores over four points.

Table 2 provides a synopsis of several studies that address this topic.

III. PROPOSED METHOD

The color green that plants reflect is one of the indicators of healthy photosynthesis [18], [20], [49]. Therefore, this study begins by filtering only the green color, extending the findings of prior research by doing so [17]. To prevent erroneous identification of plants against a bright background, a minimum saturation threshold must be established. Also, a minimum intensity (value) can be set to keep dark pixels from being wrongly labeled. It is possible to change hue, saturation, and value to fit different species [50].

In this investigation, a novel approach employing the HP technique was used to optimize the CS procedure. In the HSV, optimization is done by choosing the desired colors with the HSF, which involves setting threshold values for each hue, saturation, and value. The proposed method involves element-wise matrix multiplication utilizing the HP technique between the matrix resulting from the conversion to HSV without selection and the matrix resulting from the conversion with selection. The optimization results indicate that the desired colors have been successfully separated from other colors. By adjusting the threshold values for hue, saturation, and intensity/value, the proposed method, as depicted in FIGURE 4, can also be utilized to select various desired colors.

This is the broad outline of our methodology:

- First, an RGB image is transformed into an HSV one. This HSV conversion consists of two phases: the first, the conversion itself, is performed without any selection, and the second, the selection criteria are applied to the converted data.
- As part of the selection procedure, the hue values are filtered according to the minimum and maximum thresholds you set, as are the saturation and value. A binary matrix is used to keep track of the results of the selection process, with zeros representing pixels that did not pass muster and ones representing those that did.
- In order to obtain the final selection results, we used the HP technique, which involved multiplying each element of the binary matrix by its corresponding element in the HSV matrix that emerged as a result of the conversion performed without selection.
- We obtain the final selection results by multiplying each element of the binary matrix by its corresponding element in the HSV matrix that resulted from the conversion performed without selection. This is done utilizing the HP technique.

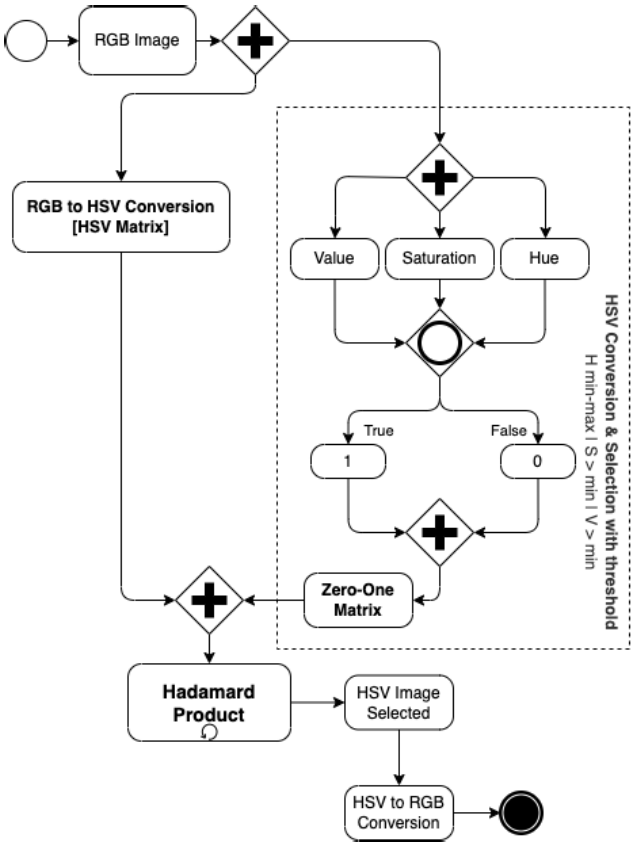

FIGURE 4. Proposed method for CS using HP technique.

A. COLOR SPACE CONVERSION

In order to separate the hue/color channel from the saturation and value channels, the RGB color space (RGB) was changed into the HSV. Due to the inconsistency of RGB images in providing color values in comparison to HSV images, color conversion was required. In FIGURE 5 and Table 3, the hue value of the green color in the RGB image varies, whereas the hue value remains constant at 120° in the HSV image. There are distinct R, G, and B values for the green hue in each of the three images, resulting in distinguishable color differences. In contrast, the hue value in the HSV remains constant while the S and V values vary.

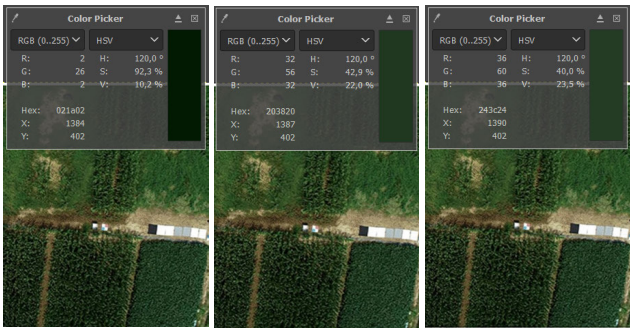

FIGURE 5. Comparison of RGB and HSV color value consistency.

The RGB image's R, G, and B values are first normalized before being converted to HSV. For each RGB image, we can get its r (1), g (2), and b (3) values by first normalizing each

TABLE 3. Comparison of RGB with HSV color value.

Image	R	G	B	H	S	V
1	2	26	2	120,0°	92,3%	10,2%
2	32	56	60	120,0°	42,9%	22,0%
3	36	60	36	120,0°	40,0%	23,5%

individual pixel [51]:

$$r = \frac{R}{R+G+B} \tag{1}$$

$$g = \frac{G}{R+G+B} \tag{2}$$

$$b = \frac{B}{R+G+B} \tag{3}$$

$$V = \max(r, g, b) \tag{4}$$

$$S = \begin{cases} 0 & \text{if } V = 0 \\ V - \frac{\min(r,g,b)}{V} & \text{if } V > 0 \end{cases} \tag{5}$$

$$H = \begin{cases} 0 & \text{if S} = 0 \\ 60° \times \left[\frac{g-b}{S \times V}\right] & \text{if V} = r \\ 60° \times \left[2 + \frac{b-r}{S \times V}\right] & \text{if } \max = g \\ 60° \times \left[4 + \frac{r-g}{S \times V}\right] & \text{if } \max = b \\ H + 360° & \text{if } H < 0 \end{cases} \tag{6}$$

B. COLOR SELECTION

CS is performed by applying the criteria where the hue value falls between the lower and upper thresholds, and then setting the lower threshold for saturation and intensity/value respectively. Using the heavy side step function, the threshold values are implemented (HSF). According to the desired color range, the hue, saturation, and value ranges of each image can be modified. The following formula can be used to express the equation for CS using the HSF:

$$\mathcal{H}(H_o - H_{min}) \tag{7}$$

$$\mathcal{H}(H_{max} - H_o) \tag{8}$$

$$H = H_o \times (\mathcal{H}(H_o - H_{min}) - \mathcal{H}(H_{max} - H_o)) \tag{9}$$

$$S_o = \mathcal{H}(S_o - S_{min}) \tag{10}$$

$$V_o = \mathcal{H}(V_o - V_{min}) \tag{11}$$

Calculating the difference between the minimum hue value (7) and the maximum hue value (8) is the first step in arriving at the desired hue range (9). (8). In the meantime, both the saturation threshold value (10) and the value threshold value (11) are independently set. The ultimate equation (12) looks like this in order to generalize the formula so that it can be applied to a wide variety of different hue, saturation, and value criteria:

$$SelectionHSV(H_o, S_o, V_o) = H_o \times (\mathcal{H}(H_o - H_{min}) - \mathcal{H}(H_{max} - H_o)) \times H(S_o - S_{min}) \times \mathcal{H}(V_o - V_{min}) \tag{12}$$

where:

$$\mathcal{H}_{(x)} = \begin{cases} 0, x < 0, \\ 1, x \geq 0 \end{cases} \tag{13}$$

$$0° \leq H_o \leq 360^0 \tag{14}$$

$$0 \leq S_o \leq 255 \tag{15}$$

$$0 \leq V_o \leq 255 \tag{16}$$

$H_{\min}$ = Hue lower threshold value
$H_{\max}$ = Hue upper threshold value
$S_{\min}$ = Saturation lower threshold value
$V_{\min}$ = Value/Intensity lower threshold value

FIGURE 6 illustrates (7), (8), and (9) that state the HSV Hue threshold values. These equations can be found in the text. In the meantime, the minimum values for the Saturation and Value thresholds can be seen depicted in FIGURE 7 and FIGURE 8 according to (10) and (11).

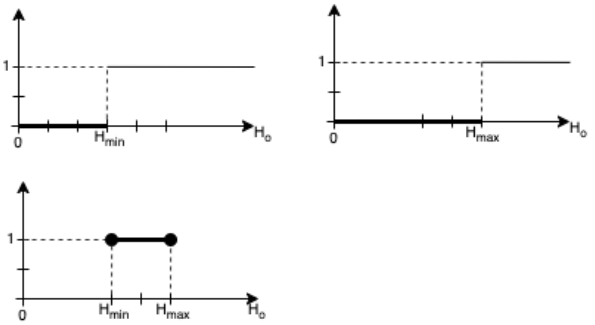

FIGURE 6. Hue threshold values.

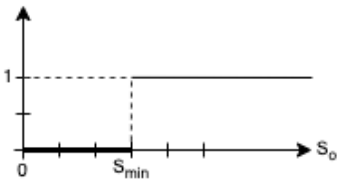

FIGURE 7. Saturation threshold value.

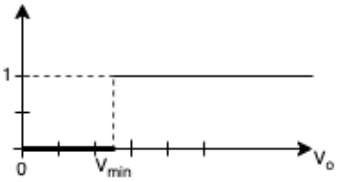

FIGURE 8. Intensity/value threshold value.

C. HADAMARD PRODUCT TECHNIQUE

The conversion results with CS are stored as zero-one matrices, while the conversion results without selection are stored

as HSV matrices. The zero-one matrix represents the outcome of CS, which serves as a mask for the original image (HSV matrix), enabling the creation of an image with the selected colors.

$$\begin{aligned}\text{Final} &= A \odot B \\ &= \begin{pmatrix} a_{11} & \cdots & a_{1n} \\ \vdots & \ddots & \vdots \\ a_{m1} & \cdots & a_{mn} \end{pmatrix} \odot \begin{pmatrix} b_{11} & \cdots & b_{1n} \\ \vdots & \ddots & \vdots \\ b_{m1} & \cdots & b_{mn} \end{pmatrix} \\ &= \begin{pmatrix} a_{11} \cdot b_{11} & \cdots & a_{1n} \cdot b_{1n} \\ \vdots & \ddots & \vdots \\ a_{m1} \cdot b_{m1} & \cdots & a_{mn} \cdot b_{mn} \end{pmatrix} \end{aligned} \tag{17}$$

Multiplication of each matrix element with the HP technique between *the zero-one* matrix and *the HSV matrix will produce an* HSV selected image (17). The image matrix of CS in the HSV is stored in the $\mathbf{A}_{(\mathbf{M},\mathbf{N})}$ matrix, while the converted image to HSV without selection is stored in the $\mathbf{B}_{(\mathbf{M},\mathbf{N})}$ matrix. The final matrix is stored on the $\mathbf{Final}_{(\mathbf{M},\mathbf{N})}$ matrix which is the HP result of$\mathbf{A}_{(\mathbf{M},\mathbf{N})} \odot \mathbf{B}_{(\mathbf{M},\mathbf{N})}$. Reverse conversion from HSV to RGB is performed so that CS results can be displayed.

IV. EXPERIMENT RESULT & DISCUSSION

The experiments were conducted on two different datasets from two previous studies [10], [17]. The first experiment aimed to assess the performance in improving computational speed, while the second experiment aimed to evaluate the accuracy and simplicity of the CS process using the proposed method.

A. EXPERIMENT I

In the initial study, an experiment was conducted to select green leaf colors from images of plants. A change from RGB to HSV was made to separate the color channels from the channels for intensity and saturation. The initial experiment involved filtering green hue values between 90 and 150. The results of the experiment demonstrated the successful separation of green leaf colors, although there were instances in which certain components of the green color were not entirely separated [17]. Incorporating two additional parameters, saturation and intensity/value, an optimization was conducted based on these experimental findings. Because the unselected green colors exhibited varying intensities and saturations, saturation and intensity were introduced as additional parameters. Experimenting with different threshold values for saturation and intensity was part of the procedure. Experiments were conducted for the selection of green colors within the wavelength range of 500 nm to 600 nm in this study. During the RGB to HSV image conversion, the green color was chosen with a hue range of 90° to 150°, saturation > 90, and intensity or value > 85.

A dataset consisting of five (five) RGB images that were captured using a visible-light camera that was mounted on a UAV was utilized in the testing of the method that was proposed. The images had a resolution of approximately 12 megapixels on average [17]. The dataset that was used for this investigation includes pictures that show a wide variety of shades and types of green vegetation. The dataset contains images that show a variety of locations and things, including roads, buildings, and other things. The varied characteristics of this dataset are put to use in an effort to improve the accuracy of the CS process.

Equation (18) used to calculate the difference in the speed of computation time. In this formula, CT will tell you how many times faster or slower the required computation time for N^b than the required computation time for O^a.

$$\mathbf{CT} = \frac{O^a}{N^b} \tag{18}$$

where:

CT : Proportion of the computation time

O^a : The computation time of the previous method is in seconds

Nb : Computation time of the proposed method in seconds

As can be seen in Table 4, the application of the proposed method results in an increase in the average computing speed of 1,078.82 times faster. This speed increase was accomplished by modifying the algorithm that was being used, moving away from looping and towards matrix element multiplication utilizing the HDP technique.

TABLE 4. Dataset.

No	Dataset	O^a	N^b	CT	H	S	V
1	North Konawe Palm Land	214,65	0,22	975,68	100-130	90	75
2	Ciwidey Cabbage Garden	223,45	0,25	893,80	80-140	60	75
3	FSRD ITB Bandung	142,40	0,15	949,33	80-140	75	75
4	ITB North Gate	262,40	0,20	1.312,00	80-140	70	70
5	Cipularang Toll Road Km 88	240,02	0,19	1.263,26	100-130	90	75
			Average	1.078,82			

The addition of selection parameters, specifically saturation and value, is the main distinction between the proposed method and the method that was previously used. This distinction is illustrated in FIGURE 9. The Hadamard product technique, which performs element-wise multiplication between the HSV matrix and the SelectedHSV matrix, is incorporated into the method that has been proposed as an addition to the use of the Hadamard product technique. The computational speed can be significantly improved using this HP method, which can make it as much as a thousand times faster.

B. EXPERIMENT II

The proposed method was also tested with the dataset from the research on Greenness Identification, which introduced an HSV decision tree-based approach requiring four steps. This was done in order to verify the accuracy of the proposed method [10]. In HSV decision tree-based research, four steps are required. To mitigate the effects of illumination, the RGB is converted to the HSV in the first step. The second step

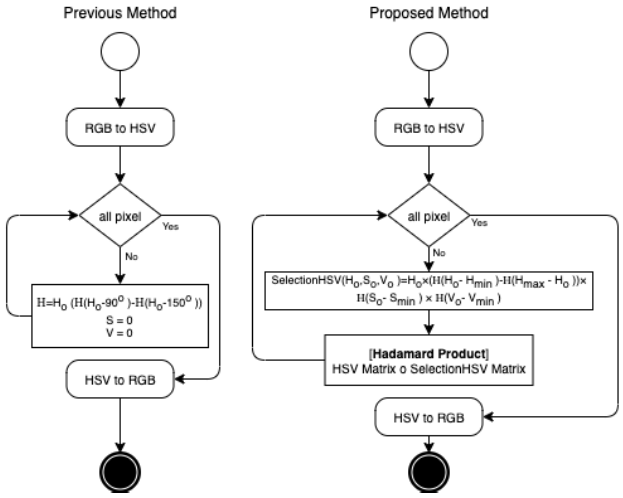

FIGURE 9. The previous method vs proposed method.

focuses on removing a significant portion of background pixels based on their hue values in comparison to those of green plants. Thirdly, pixels representing wheat straw with hue values that overlap young green leaves are eliminated based on hue, saturation, and value. In the final step, thresholding is utilized to obtain pixels that depict the greenness of corn plants.

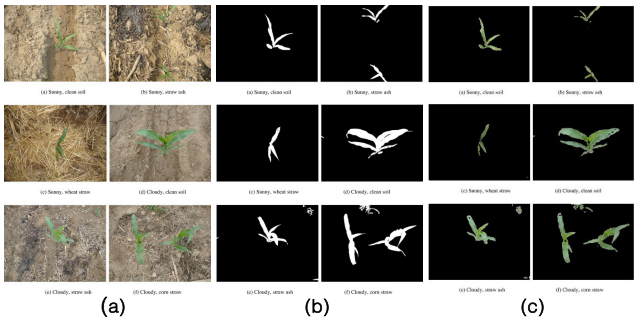

FIGURE 10. Results of the comparison of the proposed method with the HSV decision tree.

The results of the tests conducted on the proposed method for successfully selecting images of corn seedlings with a shorter process that maintains the same level of accuracy, instantly displaying the color green that they have, are depicted in FIGURE 10. This figure shows the results of the tests conducted on the proposed method. FIGURE 10(a) depicts an image of corn seedlings growing amongst straw, FIGURE 10(b) depicts the CS results using the HSV-Tree method, and FIGURE 10(c) depicts the CS results using the proposed method. When utilizing the suggested approach, the necessary amount of time for processing is 0.009582 seconds when utilizing the given parameters H_{min} =70; H_{max} = 125, S_{min} = 15 dan V_{min} = 100.

The differences between the approaches that were taken are depicted in FIGURE 11, which demonstrates that the method that was suggested is not only quicker, but it also

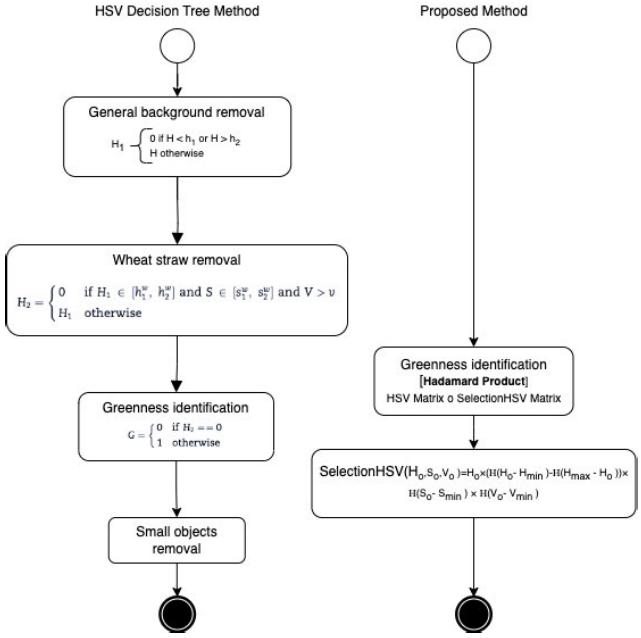

FIGURE 11. The HSV-decission tree method vs proposed method.

does not require the removal of the background or the straw. The results can be relied on to be accurate when using the method that has been proposed, which also features an accelerated procedure while directly displaying the desired shade of green.

It is apparent from both experiments that the suggested approach can be operationalized to sort colors according to the intended hue. By utilizing the HDP technique, the proposed method for color sorting can decrease computation time and obviates the need for feature extraction. Additionally, the proposed method exhibits exceptional computational speed, rendering it suitable for subsequent investigations concerning the utilization of UAVs for real-time color selection.

V. CONCLUSION

By incorporating the parameters Saturation and Value, this research was able to successfully optimize the process of selecting a green color within the wavelength range of 500 nm to 600 nm or the hue range of 90° to 150°. This was accomplished within the context of the study. During the process of converting from the RGB to the HSV, the optimization was carried out with the help of the HSF technique and the HDP method. The optimization resulted in a significant improvement to the process of selecting colors by completely filtering out colors that were not desired. With the workflow being streamlined and the computational speed having been increased 1,078.82 times faster, the HSV CS computation is now significantly faster than it was before. This strategy for optimizing the CS process can be applied not only to the selection of the green color but also to the selection of any other color.

CONFLICT OF INTEREST

The authors of this paper have stated that there are no conflicts of interest associated with it.

REFERENCES

[1] F. J. López-Rubio, E. Domínguez, E. J. Palomo, E. López-Rubio, and R. M. Luque-Baena, "Selecting the color space for self-organizing map based foreground detection in video," *Neural Process. Lett.*, vol. 43, no. 2, pp. 345–361, Apr. 2016, doi: 10.1007/s11063-015-9431-8.

[2] J. Fan, "Intelligent colour selection method for product packaging design based on particle swarm optimisation," *Int. J. Manuf. Technol. Manage.*, vol. 37, no. 2, pp. 162–172, 2023, doi: 10.1504/ijmtm.2023.131303.

[3] A. Radonjić, N. P. Cottaris, and D. H. Brainard, "The relative contribution of color and material in object selection," *PLOS Comput. Biol.*, vol. 15, no. 4, Apr. 2019, Art. no. e1006950, doi: 10.1371/journal.pcbi.1006950.

[4] M. A. Ansari and D. K. Singh, "Significance of color spaces and their selection for image processing: A survey," *Recent Adv. Comput. Sci. Commun.*, vol. 15, no. 7, Sep. 2022, Art. no. e190522192129, doi: 10.2174/2666255814666210308152108.

[5] L. Maulana, Y. G. Bihanda, and Y. A. Sari, "Color space and color channel selection on image segmentation of food images," *Register, Jurnal Ilmiah Teknologi Sistem Informasi*, vol. 6, no. 2, p. 141, Sep. 2020, doi: 10.26594/register.v6i2.2061.

[6] G. L. Cole and J. A. Endler, "Artificial selection for food colour preferences," *Proc. Roy. Soc. B, Biol. Sci.*, vol. 282, no. 1804, Apr. 2015, Art. no. 20143108, doi: 10.1098/rspb.2014.3108.

[7] W. Li, Z. Zhang, M. Wang, and H. Chen, "Fabric defect detection algorithm based on image saliency region and similarity location," *Electronics*, vol. 12, no. 6, p. 1392, Mar. 2023, doi: 10.3390/electronics12061392.

[8] O. A. L. F. Pimentel, A. M. Amado, and N. H. They, "Biofloc colors as an assessment tool for water quality in shrimp farming with BFT systems," *Aquacultural Eng.*, vol. 101, May 2023, Art. no. 102321, doi: 10.1016/j.aquaeng.2023.102321.

[9] M. Yum, "Digital image color analysis method to extract fashion color semantics from artworks," *Multimedia Tools Appl.*, vol. 82, no. 11, pp. 17115–17133, May 2023, doi: 10.1007/s11042-022-14189-w.

[10] W. Yang, S. Wang, X. Zhao, J. Zhang, and J. Feng, "Greenness identification based on HSV decision tree," *Inf. Process. Agricult.*, vol. 2, nos. 3–4, pp. 149–160, Oct. 2015, doi: 10.1016/j.inpa.2015.07.003.

[11] J. Venetis, "An explicit expression of the unit step function," *Int. Rev. Electr. Eng. (IREE)*, vol. 18, no. 1, p. 83, Feb. 2023, doi: 10.15866/iree.v18i1.23117.

[12] H. Deng, B. Yan, X. Zhang, Y. Zhu, and J. Koyanagi, "New crack front enrichment for XFEM modeling," *Int. J. Solids Struct.*, vol. 274, Jul. 2023, Art. no. 112280, doi: 10.1016/j.ijsolstr.2023.112280.

[13] L. Huo and Y. Yu, "The impact of the self-recognition ability and physical quality on coupled negative information-behavior-epidemic dynamics in multiplex networks," *Chaos, Solitons Fractals*, vol. 169, Apr. 2023, Art. no. 113229, doi: 10.1016/j.chaos.2023.113229.

[14] W. Jiang and H. Hu, "Hadamard product perceptron attention for image captioning," *Neural Process. Lett.*, vol. 55, no. 3, pp. 2707–2724, Jun. 2023, doi: 10.1007/s11063-022-10980-w.

[15] P.-H. Wu, Y.-P. Lan, C.-L. Chou, and C.-T. Lin, "Fast infrared small target detection by using Hadamard product for spatial–temporal matrices," *IEEE Access*, vol. 10, pp. 116830–116843, 2022, doi: 10.1109/ACCESS.2022.3215851.

[16] Z. Yang, P. Stoica, and J. Tang, "Source resolvability of spatial-smoothing-based subspace methods: A Hadamard product perspective," *IEEE Trans. Signal Process.*, vol. 67, no. 10, pp. 2543–2553, May 2019, doi: 10.1109/TSP.2019.2908142.

[17] T. Kusnandar, J. Santoso, and K. Surendro. (Jun. 2023). *Modification Color Filtering in HSV Color Space*. [Online]. Available: http://dx.doi.org/10.21203/rs.3.rs-2650337/v1

[18] A. R. Huete, "Remote sensing for environmental monitoring," in *Environmental Monitoring and Characterization*. Amsterdam, The Netherlands: Elsevier, 2004, pp. 183–206, doi: 10.1016/B978-012064477-3/50013-8.

[19] K. Jack, "Color spaces," in *Video Demystified*. Elsevier, Jan. 2007, pp. 15–36, doi: 10.1016/B978-075068395-1/50003-1.

[20] H. L. Smith, L. McAusland, and E. H. Murchie, "Don't ignore the green light: Exploring diverse roles in plant processes," *J. Experim. Botany*, vol. 68, no. 9, pp. 2099–2110, Apr. 2017, doi: 10.1093/jxb/erx098.

[21] A. Gijsenij, T. Gevers, and J. van de Weijer, "Computational color constancy: Survey and experiments," *IEEE Trans. Image Process.*, vol. 20, no. 9, pp. 2475–2489, Sep. 2011.

[22] A. K. Bhunia, G. Kumar, P. P. Roy, R. Balasubramanian, and U. Pal, "Text recognition in scene image and video frame using color channel selection," *Multimedia Tools Appl.*, vol. 77, no. 7, pp. 8551–8578, Apr. 2018, doi: 10.1007/s11042-017-4750-6.

[23] A. Patrignani and T. E. Ochsner, "Canopeo: A powerful new tool for measuring fractional green canopy cover," *Agronomy J.*, vol. 107, no. 6, pp. 2312–2320, Nov. 2015, doi: 10.2134/agronj15.0150.

[24] J. I. Córcoles, J. F. Ortega, D. Hernández, and M. A. Moreno, "Estimation of leaf area index in onion (Allium cepa L.) using an unmanned aerial vehicle," *Biosystems Eng.*, vol. 115, no. 1, pp. 31–42, May 2013, doi: 10.1016/j.biosystemseng.2013.02.002.

[25] A. Agapiou, "Vegetation extraction using visible-bands from openly licensed unmanned aerial vehicle imagery," *Drones*, vol. 4, no. 2, p. 27, Jun. 2020, doi: 10.3390/drones4020027.

[26] Y. Wang, Z. Yang, G. Kootstra, and H. A. Khan, "The impact of variable illumination on vegetation indices and evaluation of illumination correction methods on chlorophyll content estimation using UAV imagery," *Plant Methods*, vol. 19, no. 1, p. 51, May 2023, doi: 10.1186/s13007-023-01028-8.

[27] M. H. AlRowaily, H. Arof, and I. Ibrahim, "Luminosity and contrast adjustment of fundus images with reflectance," *Appl. Sci.*, vol. 13, no. 5, p. 3312, Mar. 2023, doi: 10.3390/app13053312.

[28] J. Best, *Colour Design: Theories and Applications* (The Textile Institute Book Series), 2nd ed. Cambridge, MA, USA: Elsevier, 2017.

[29] P. J. Marlow, J. Kim, and B. L. Anderson, "The perception and misperception of specular surface reflectance," *Current Biol.*, vol. 22, no. 20, pp. 1909–1913, Oct. 2012, doi: 10.1016/j.cub.2012.08.009.

[30] R. A. Jayashree, "RGB to HSI color space conversion via MACT algorithm," in *Proc. Int. Conf. Commun. Signal Process.* Melmaruvathur, India: IEEE, Apr. 2013, pp. 561–565, doi: 10.1109/iccsp.2013.6577117.

[31] Q. Zhang and S.-I. Kamata, "A novel color space based on RGB color barycenter," in *Proc. IEEE Int. Conf. Acoust., Speech Signal Process. (ICASSP)*, Shanghai, Mar. 2016, pp. 1601–1605, doi: 10.1109/ICASSP.2016.7471947.

[32] C. Lau, W. Heidrich, and R. Mantiuk, "Cluster-based color space optimizations," in *Proc. Int. Conf. Comput. Vis.* Barcelona, Spain, Nov. 2011, pp. 1172–1179, doi: 10.1109/ICCV.2011.6126366.

[33] S. K. Naik and C. A. Murthy, "Hue-preserving color image enhancement without gamut problem," *IEEE Trans. Image Process.*, vol. 12, no. 12, pp. 1591–1598, Dec. 2003, doi: 10.1109/tip.2003.819231.

[34] S. Sivavelu and V. Palanisamy, "Gaussian kernelized feature selection and improved multilayer perceptive deep learning classifier for software fault prediction," *Indonesian J. Electr. Eng. Comput. Sci.*, vol. 30, no. 3, p. 1534, Jun. 2023, doi: 10.11591/ijeecs.v30.i3.pp1534-1547.

[35] A. Guo, W. Huang, H. Ye, Y. Dong, H. Ma, Y. Ren, and C. Ruan, "Identification of wheat yellow rust using spectral and texture features of hyperspectral images," *Remote Sens.*, vol. 12, no. 9, p. 1419, Apr. 2020, doi: 10.3390/rs12091419.

[36] G. X. Ritter and H. Zhu, "The generalized matrix product and its applications," *J. Math. Imag. Vis.*, vol. 1, no. 3, pp. 201–213, Sep. 1992, doi: 10.1007/bf00129875.

[37] B. Maxfield, "Arrays, vectors, and matrices," in *Essential Mathcad for Engineering, Science, and Math*. Amsterdam, The Netherlands: Elsevier, 2009, pp. 101–128, doi: 10.1016/B978-0-12-374783-9.00005-9.

[38] G. P. H. Styan, "Hadamard products and multivariate statistical analysis," *Linear Algebra Appl.*, vol. 6, pp. 217–240, Jan. 1973, doi: 10.1016/0024-3795(73)90023-2.

[39] S. Liu, V. Leiva, D. Zhuang, T. Ma, and J. I. Figueroa-Zúñiga, "Matrix differential calculus with applications in the multivariate linear model and its diagnostics," *J. Multivariate Anal.*, vol. 188, Mar. 2022, Art. no. 104849, doi: 10.1016/j.jmva.2021.104849.

[40] X. Liu, Y. Zou, and X. Yan, "A new model of the harmonic control based on Hadamard product," *J. Control Theory Appl.*, vol. 7, no. 4, pp. 433–437, Nov. 2009, doi: 10.1007/s11768-009-7235-y.

[41] R. Liu, S. Li, J. Liu, L. Ma, X. Fan, and Z. Luo, "Learning Hadamard-product-propagation for image dehazing and beyond," *IEEE Trans. Circuits Syst. Video Technol.*, vol. 31, no. 4, pp. 1366–1379, Apr. 2021, doi: 10.1109/TCSVT.2020.3004854.
[42] S. Omran, I. Masmali, and G. Alhamzi, "Banach fixed point theorems in generalized metric space endowed with the Hadamard product," *Symmetry*, vol. 15, no. 7, p. 1325, Jun. 2023, doi: 10.3390/sym15071325.
[43] D. Yang, J. Li, X. Zhang, and H. Liu, "Simultaneous estimation of 2-DOF wrist movements based on constrained non-negative matrix factorization and Hadamard product," *Biomed. Signal Process. Control*, vol. 56, Feb. 2020, Art. no. 101729, doi: 10.1016/j.bspc.2019.101729.
[44] J. Oakes and M. Balota, "Distinguishing plant population and variety with UAV-derived vegetation indices," in *Proc. SPIE*, J. A. Thomasson, M. McKee, and R. J. Moorhead, Eds. Anaheim, CA, USA, May 2017, Art. no. 102180G, doi: 10.1117/12.2262631.
[45] A. N. Jasim, L. C. Fourati, and O. S. Albahri, "Evaluation of unmanned aerial vehicles for precision agriculture based on integrated fuzzy decision-making approach," *IEEE Access*, vol. 11, pp. 75037–75062, 2023, doi: 10.1109/ACCESS.2023.3294094.
[46] P. K. R. Maddikunta, S. Hakak, M. Alazab, S. Bhattacharya, T. R. Gadekallu, W. Z. Khan, and Q.-V. Pham, "Unmanned aerial vehicles in smart agriculture: Applications, requirements, and challenges," *IEEE Sensors J.*, vol. 21, no. 16, pp. 17608–17619, Aug. 2021, doi: 10.1109/JSEN.2021.3049471.
[47] H. L. Vigne, G. Charron, S. Hovington, and A. L. Desbiens, "Assisted canopy sampling using unmanned aerial vehicles (UAVs)," in *Proc. Int. Conf. Unmanned Aircr. Syst. (ICUAS)*. Athens, Greece: IEEE, Jun. 2021, pp. 1642–1647, doi: 10.1109/ICUAS51884.2021.9476818.
[48] G. Weil, I. Lensky, Y. Resheff, and N. Levin, "Optimizing the timing of unmanned aerial vehicle image acquisition for applied mapping of woody vegetation species using feature selection," *Remote Sens.*, vol. 9, no. 11, p. 1130, Nov. 2017, doi: 10.3390/rs9111130.
[49] R. H. Grant, "Partitioning of biologically active radiation in plant canopies," *Int. J. Biometeorology*, vol. 40, no. 1, pp. 26–40, Feb. 1997, doi: 10.1007/bf02439408.
[50] T. Wang, A. Chandra, J. Jung, and A. Chang, "UAV remote sensing based estimation of green cover during turfgrass establishment," *Comput. Electron. Agricult.*, vol. 194, Mar. 2022, Art. no. 106721, doi: 10.1016/j.compag.2022.106721.
[51] L.-S. Yu, S.-Y. Chou, H.-Y. Wu, Y.-C. Chen, and Y.-H. Chen, "Rapid and semi-quantitative colorimetric loop-mediated isothermal amplification detection of ASFV via HSV color model transformation," *J. Microbiology, Immunology Infection*, vol. 54, no. 5, pp. 963–970, Oct. 2021, doi: 10.1016/j.jmii.2020.08.003.

TONI KUSNANDAR received the Bachelor of Economics degree in management from the INABA College of Economics, Bandung, Indonesia, in 1994, and the Master of Engineering degree in informatics from the School of Electrical and Informatics Engineering (STEI), Institut Teknologi Bandung (ITB), Bandung, in 2013, where he is currently pursuing the Ph.D. degree with STEI. He joined STMIK Mardira Indonesia, in 2008. His research interests include image processing, information systems, and data science.

JUDHI SANTOSO received the B.Eng. degree from the Institut Teknologi Bandung (ITB), Indonesia, in 1987, the master's degree from Universitas Indonesia, Jakarta, Indonesia, in 1991, and the Ph.D. degree from ITB, in 2006. He is currently an Associate Professor in computer science with ITB. His research interests include computer graphics and computer-aided design, theoretical computer science, and computer science.

KRIDANTO SURENDRO (Member, IEEE) received the B.Eng. and master's degrees in industrial engineering from the Institut Teknologi Bandung (ITB), Indonesia, in 1987 and 1991, respectively, and the Ph.D. degree in computer science from Keio University, Japan, in 1999. He is currently a Professor in computer science with ITB. His research interests include data science, soft computing, and IT governance.